Engineering and Modeling the Electrophoretic Trapping of a Single Protein Inside a Nanopore

Willems, Kherim; Ruić, Dino; Biesemans, Annemie; Galenkamp, Nicole Stéphanie; Van Dorpe, Pol; Maglia, Giovanni

Published in:
Acs Nano

DOI:
10.1021/acsnano.8b09137

Publication date:
2019

ACS NANO

Cite This: ACS Nano 2019, 13, 9980−9992

www.acsnano.org

ARTICLE

Engineering and Modeling the Electrophoretic Trapping of a Single Protein Inside a Nanopore

Kherim Willems,[†,‡,⊥] Dino Ruić,[‡,§,⊥] Annemie Biesemans,[†,⊥] Nicole Stéphanie Galenkamp,[∥] Pol Van Dorpe,[‡,§] and Giovanni Maglia*[,∥]

[†]Department of Chemistry, KU Leuven, Celestijnenlaan 200F, B-3001 Leuven, Belgium

[‡]imec, Kapeldreef 75, B-3001 Leuven, Belgium

[§]Department of Physics and Astronomy, KU Leuven, Celestijnenlaan 200D, B-3001 Leuven, Belgium

[∥]Groningen Biomolecular Sciences & Biotechnology Institute, University of Groningen, 9747 AG Groningen, The Netherlands

Supporting Information

ABSTRACT: The ability to confine and to study single molecules has enabled important advances in natural and applied sciences. Recently, we have shown that unlabeled proteins can be confined inside the biological nanopore Cytolysin A (ClyA) and conformational changes monitored by ionic current recordings. However, trapping small proteins remains a challenge. Here, we describe a system where steric, electrostatic, electrophoretic, and electro-osmotic forces are exploited to immobilize a small protein, dihydrofolate reductase (DHFR), inside ClyA. Assisted by electrostatic simulations, we show that the dwell time of DHFR inside ClyA can be increased by orders of magnitude (from milliseconds to seconds) by manipulation of the DHFR charge distribution. Further, we describe a physical model that includes a double energy barrier and the main electrophoretic components for trapping DHFR inside the nanopore. Simultaneous fits to the voltage dependence of the dwell times allowed direct estimates of the *cis* and *trans* translocation probabilities, the mean dwell time, and the force exerted by the electro-osmotic flow on the protein (≅9 pN at −50 mV) to be retrieved. The observed binding of NADPH to the trapped DHFR molecules suggested that the engineered proteins remained folded and functional inside ClyA. Contact-free confinement of single proteins inside nanopores can be employed for the manipulation and localized delivery of individual proteins and will have further applications in single-molecule analyte sensing and enzymology studies.

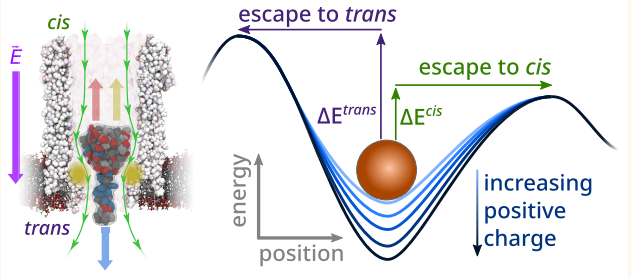

KEYWORDS: *ClyA nanopore, DHFR, electrostatic trap, electro-osmotic flow, protein electrostatics, nanomanipulation, single-molecule enzymology*

Sensors capable of the label-free interrogation of proteins at the single-molecule level have applications in biosensing, biophysics, and enzymology.[1−3] In particular, the ability to observe the behavior of individual proteins allows one to directly retrieve the rates of kinetic processes and provides a wealth of mechanistic, energetic, and structural information, which are not readily obtained from statistically averaged ensemble (bulk) measurements.[1] To achieve single-molecular sensitivity at high signal-to-noise ratios, the observational volume of the sensor should be similar in size to the object of interest (*i.e.*, zeptoliter range for a protein with a radius of 2.5 nm). Moreover, many kinetic processes have relatively long time scales (*e.g.*, 10^{-3} to 1 s) which, in turn, necessitate long observational times to obtain a statistically relevant number of events. Hence, the protein must also remain inside the observational volume for seconds or minutes, a feat that is only possible if the protein is either physically immobilized or trapped in a local energetic minimum that is significantly deeper than the thermal energy.[4,5]

To counteract the random thermal motion of nanoscale objects in solution, several optical, microfluidic, and nanofluidic methodologies have been developed over the years. The optical trapping of nanoscale objects (<50 nm radius) requires the sub-diffraction-limited confinement of light,[6−8] which can be achieved with photonic[9,10] or plasmonic[11−18] nanostructures. Although optical techniques have been shown to be capable of trapping proteins with a radius of ≈2.3 nm,[15] the

Received: December 2, 2018
Accepted: August 12, 2019
Published: August 12, 2019

DOI: 10.1021/acsnano.8b09137
ACS Nano 2019, 13, 9980−9992

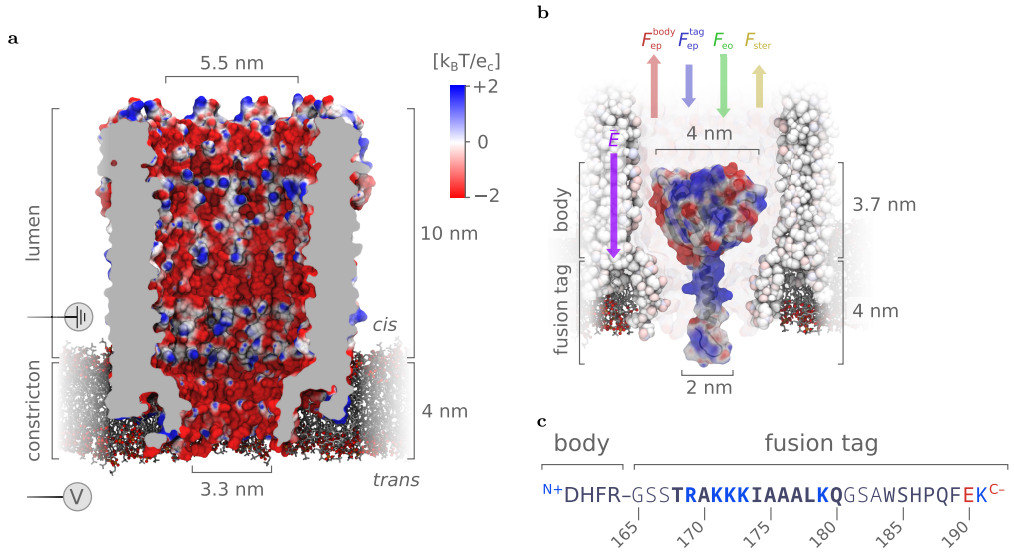

Figure 1. Trapping of proteins inside the ClyA-AS nanopore. (a) Surface representation of a type I ClyA-AS nanopore—a dodecameric version of the Cytolysin A pore containing eight mutations (C87A, L99Q, E103G, F166Y, I203V, C285S, K294R, H307Y) compared to the wild-type variant from *Salmonella typhimurium*— embedded in a planar lipid bilayer. The structure was derived through homology modeling from the wild-type crystal structure (PDB ID: 2WCD[56]) using the MODELLER,[57] VMD,[58] and NAMD[59] software packages.[60] The surface of the pore is colored according to its electrostatic potential in 150 mM NaCl, as calculated by APBS.[61−63] (b) Depiction of a single dihydrofolate reductase (DHFR) molecule extended with a positively charged C-terminal polypeptide tag ($DHFR_4S$) inside a ClyA-AS nanopore. The secondary structure of the tag (primarily α-helical) was predicted by the PEP-FOLD server.[64,65] At negative applied bias voltages relative to *trans*, the electric field (E) is expected to pull the negatively charged body of DHFR upward (F_{ep}^{body}) and the positively charged fusion tag downward (F_{ep}^{tag}), while the electro-osmotic flow pushes the entire protein downward (F_{eo}). Lastly, as the body of DHFR is larger than the diameter of the *trans* constriction, the force required to overcome the steric hindrance (F_{ster}) during full *cis*-to-*trans* translocation is expected to be significant. (c) Sequence of $DHFR_4S$ fusion tag with its positive and negative residues colored blue and red, respectively. The sequence of the Strep-tag starts at residue 183, and the GSS and GSA linkers are shown in light font. Note that, at pH 7.5, the C- and N-termini contribute one negative charge to the body and one positive charge to the tag, respectively. Images were rendered using VMD.[58,66]

high optical intensities required and the solid-state nature of the devices tend to not only trap the proteins but also unfold them, limiting the scope of their applicability.[13,18]

Microfluidic techniques might offer softer alternatives for the immobilization of single molecules. The anti-Brownian electrokinetic (ABEL) trap makes use of optical tracking to electrophoretically counteract the Brownian motion of individual dielectric particles,[19−22] enabling the trapping of proteins down to ≈2.9 nm radius[22] and even single fluorophores.[23] Because this technique uses fluorescence microscopy to track the movement of their targets, the observational time window is ultimately limited by the photobleaching of the dye.[19,21]

Nanopores, which are nanometer-sized apertures in a membrane separating two electrolyte reservoirs, have been used extensively to study single molecules.[3,24−26] In nanopore analyses, an electric field is applied across the membrane and information about a molecule passing through the pore is collected by monitoring the modulations of the ionic charge current. As proteins typically transit the pore at high velocities ($\approx 10^{-3}$ to 10^{-2} m·s^{-1}),[27−30] the dwell time (*i.e.*, the duration a molecule of interest spends inside the observable volume) is on the order of 10^{-6} to 10^{-3} s. These time scales have proven sufficient for obtaining structural information such as protein size, shape, charge, dipole moment, and rigidity,[27,30−33] but they are too brief to efficiently study the enzymatic cycle of the majority of human enzymes (turnover numbers between 10^{-3} and 10^{3} s^{-1}).

To increase the observation window of proteins by nanopores, researchers have made extensive use of noncovalent interactions. By coating solid-state nanopores with nitrilotriacetic acid (NTA) receptors, the dwell time of His-tagged proteins could be prolonged up to 6 orders of magnitude.[34] In another account, the diffusion coefficient of several proteins was reduced 10-fold *via* tethering to a lipid-bilayer-coated nanopore.[35,36] The decoration of biological nanopores with thrombin-specific aptamers enabled the investigation of the binding kinetics of thrombin to its aptamer[37] and the selective detection in the presence of a 100-fold excess of noncognate proteins.[38] Electrophoretic translocation of protein−DNA complexes through small nanopores (<3 nm diameter) typically results in the temporary trapping of the entire complex, which has allowed for the study of polymerase enzymes[39,40] and DNA-binding proteins.[41,42] Although promising, none of these approaches could efficiently control the trapping of the protein inside the nanopore or allow observation of enzyme kinetics or ligand-induced conformational changes.

The energetic landscape of a protein translocating through a nanopore stems directly from the electrostatic, electrophoretic, electro-osmotic, and steric forces exerted on it.[43] Given the relatively high motility of proteins, the creation of a long lasting (10−100 s), contact-free trap within a spatial region of a few nanometers mandates the presence of a deep potential energy well within the nanopore.[44] Such a potential profile was achieved by Luchian and co-workers, who showed that the dwell time of a polypeptide inside the α-hemolysin pore could be significantly increased by manipulating the strength of the electro-osmotic flow[45,46] or by placement of oppositely charged amino acids at the polypeptide's termini.[47] In a

DOI: 10.1021/acsnano.8b09137
ACS Nano 2019, 13, 9980−9992

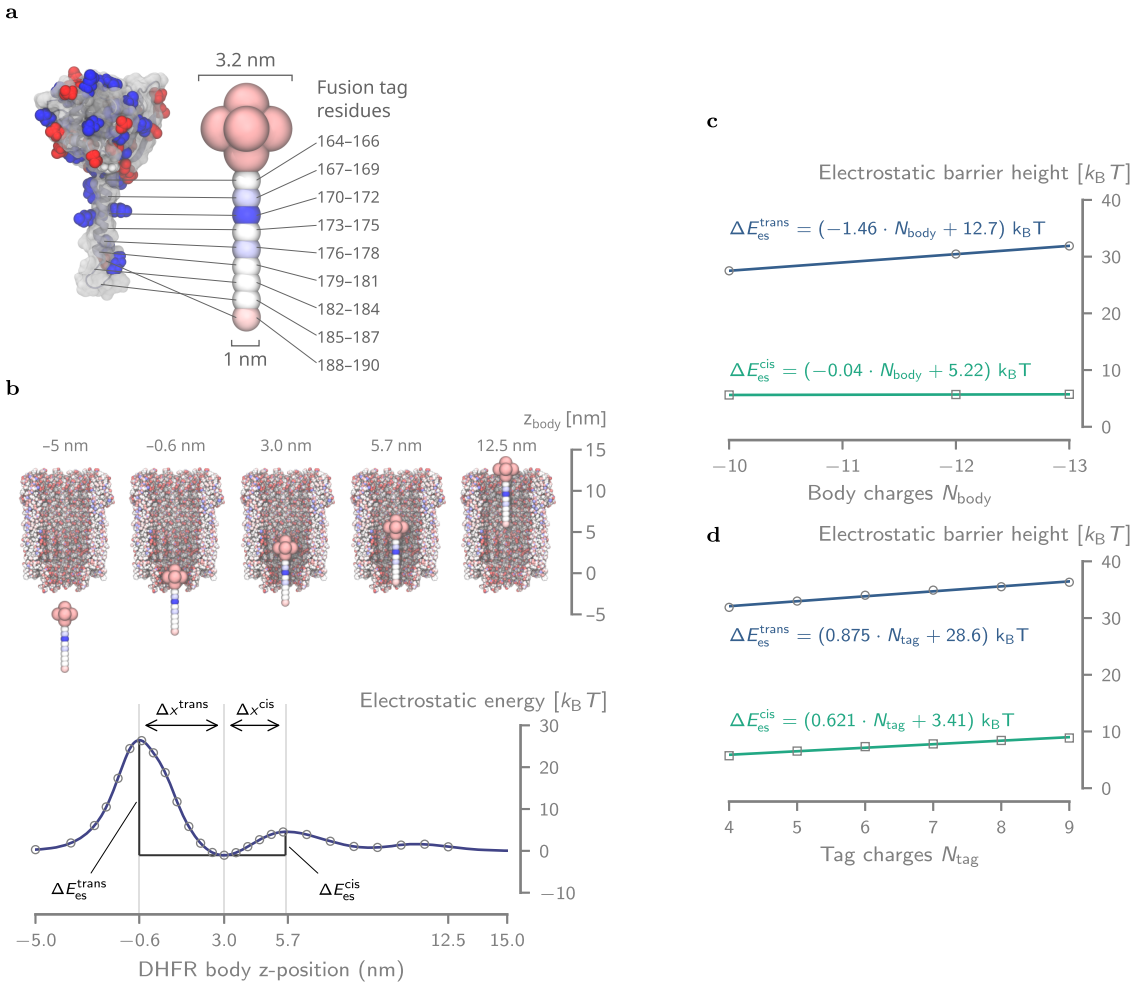

Figure 2. Energy landscape of $DHFR_4S$ inside ClyA. (a) Coarse-grained model of $DHFR_4S$ used in the electrostatic energy calculations in APBS. The body of DHFR consists of seven negatively charged (−1.43 *e*) beads (1.6 nm diameter) in a spherical configuration (0.8 nm spacing), whereas the tail is represented by a linear string of beads (1 nm diameter, 0.6 nm spacing), each holding the net charge of three amino acids. (b) Electrostatic energy (ΔE_{es}) resulting from a series of APBS energy calculations where the coarse-grained $DHFR_4S$ bead model is moved along the central axis of the pore. The distances Δx^{cis} and Δx^{trans} refer to the distances between the energy minimum near the bottom of the lumen (z = 3 nm) and the maximum at, respectively, *cis* (z = 5.7 nm) and *trans* (z = 0.6 nm). (c) Although every additional negative charge to the body of DHFR increases the *trans* electrostatic barrier by 1.46 k_BT, it has virtually no effect on the *cis* barrier, which increases only by 0.04 k_BT per charge. (d) Addition of a single positive charge to DHFR's tag affects the height of the *trans* and *cis* much more similarly, with increases of 0.875 k_BT and 0.621 k_BT per charge, respectively.

similar approach, a single barnase enzyme was trapped inside *α*-hemolysin *via* the addition of a positively charged N-terminal tag.[48]

Previous work in the Maglia group on protein analysis with nanopores was centered around the biological nanopore Cytolysin A (ClyA)—a protein with a highly negatively charged interior whose shape can best be described by a large (≈5.5 nm diameter, ≈10 nm height, *cis lumen*) and a small (≈3.3 nm diameter, ≈4 nm height, *trans constriction*) cylinder stacked on top of each other (Figure 1a).[38,49] Upon capture from the *cis* side of the pore, certain proteins exhibited exceptionally long dwell times inside ClyA from seconds up to tens of minutes,[38,49−53] enabling the monitoring of conformational changes[53−55] and even of the orientation[54] of the proteins inside the nanopore. A subset of the investigated proteins, such as lysozyme, Dendra2_M159A, and dihydrofolate reductase (DHFR), resided inside the nanopore lumen only for hundreds of microseconds and hence could not be studied.[38,50] It was observed that the size of the nanopore plays a crucial role in the effectiveness of protein trapping, as a mere <10% increase of ClyA's diameter (*i.e.*, by using ClyA nanopores with a higher oligomeric state) is enough to reduce the dwell time of proteins by almost 3 orders of magnitude.[49] Next to pore size, the charge distribution of proteins can significantly affect their dwell time inside a nanopore. For example, the binding of the negatively charged (−2 *e*) inhibitor methotrexate (MTX) to a modified DHFR molecule with a positively charged fusion tag at the C-terminus ($DHFR_{tag}$) increased the dwell time of the protein inside the ClyA nanopore from ≈3 ms to ≈3 s at −90 mV.[50]

In this work, the immobilization of individual *Escherichia coli* DHFR molecules (Figure 1b) inside the ClyA biological nanopore (specifically type I ClyA-AS,[49] Figure 1a) is investigated in detail. Using nanoscale protein electrostatic simulations as a guideline, our results show that the dwell time of $DHFR_4S$—a molecule identical to the above-mentioned $DHFR_{tag}$ aside from the insertion of a single alanine residue at its fusion tag (A174_A175insA, Figure 1c)—inside ClyA can be increased several orders of magnitude by manipulating the distribution of positive and negative charges on its surface. To

DOI: 10.1021/acsnano.8b09137
ACS Nano 2019, 13, 9980−9992

elucidate the physical origin of the trapping mechanism, a double energy barrier model was developed which—by fitting the voltage dependency of the dwell times for various DHFR mutants—yields direct estimates of the *cis* and *trans* translocation rates and the magnitude of force exerted by the electro-osmotic flow on DHFR. Our method provides an efficient means to increase the dwell time of the DHFR protein inside the ClyA nanopore and suggests a general mechanism to tune the dwell time of other proteins, which we believe has significant value for single-molecule sensing and analysis applications.

RESULTS AND DISCUSSION

Phenomenology of DHFR Trapped Inside ClyA. To effectively study the enzymes at the single-molecular level, one must be able to collect a statistically significant number (*i.e.*, typically hundreds) of catalytic cycles from the same enzyme. In the case of the *E. coli* DHFR, which has a turnover number of ≈0.08 s,[67] this means that the protein must remain trapped inside the pore for tens of seconds. However, as detailed above, such long dwell times were only achieved for DHFR by adding a positively charged polypeptide tag to the C-terminus of DHFR, together with the binding of the negatively charged inhibitor methotrexate (MTX).[50] Although these long dwell times are encouraging, the requirement for MTX excludes the study of the full enzymatic cycle. Hence, using these previous findings as a starting point, we aim to find out how to prolong the dwell time of a tagged DHFR molecule inside the ClyA-AS nanopore without the use of MTX and to understand the fundamental physical mechanisms that determine the escape of DHFR from the pore.

The structure of $DHFR_4S$, the tagged DHFR molecule used as a starting point in this work, can be roughly divided into a "body", which encompasses the enzyme itself and has a net negative charge, $N_{body} = -10\ e$, and a "tag", which comprises the C-terminal polypeptide extension and bears a net positive charge, $N_{tag} = +4\ e$ (Figure 1b,c). To capture a tagged DHFR molecule, an electric field oriented from *cis* to *trans* (*i.e.*, negative bias voltage) must be applied across the nanopore, which gives rise to an electro-osmotic flow pushing the protein into the pore (F_{eo}). The electrophoretic force on the body (F_{ep}^{body}) strongly opposes this electro-osmotic force but is significantly weakened by the electrophoretic force on the tag (F_{ep}^{tag}), allowing the protein to be captured.[38,50,55] As the body and tag of the DHFR molecules bear a significant amount of opposing charges, it is likely that the molecule will align itself with the electric field, where the tag is oriented toward the *trans* side. In this configuration, the body sits in the ClyA lumen and the tag is located in or near the narrow constriction. Because the body (≈4 nm) is larger than the diameter of the constriction (3.3 nm), the steric hindrance between the body and the pore is expected to strongly disfavor full translocation to the *trans* reservoir, giving rise to an apparent "steric hindrance" force (F_{ster}). Finally, Poisson−Boltzman electrostatic calculations calculations showed that the negatively charged interior of ClyA-AS creates a negative electrostatic potential within both the lumen ($\approx -0.3\ k_BT/e$) and the constriction ($\approx -1\ k_BT/e$) of the pore,[60] which will result in disfavorable and favorable interactions with the body and the tag, respectively.

Energy Landscape of DHFR in ClyA. To increase the dwell time of DHFR—and to generalize our findings for other proteins—it is necessary to understand how the forces exerted on DHFR inside the pore behave as a function of the experimental conditions (*e.g.*, charge distribution and applied bias). In the absence of specific high affinity interactions, DHFR's trapping behavior should be chiefly determined by its electrostatic interactions with the pore, whereas the external electrophoretic and electro-osmotic forces can be viewed as modifications thereof. Hence, we will start by investigating the molecule's electrostatic energy landscape within ClyA in equilibrium where the externally applied electric field vanishes.

To this end, we used the adaptive Poisson−Boltzmann solver (APBS) to compute the electrostatic energy of a simplified bead-like-tagged DHFR molecule model as it moves through the pore (Figure 2a,b; see Supporting Information section 2 for details).[61−63,68] The bead-like model was chosen such that its body's size is small enough to pass the constriction without necessitating conformational changes as these cannot be modeled using APBS. Hence, this also means that the magnitude of maxima of the electrostatic energy landscape, which occur when the bead model's charges come close to the pore's charges, should be viewed as indicative and not absolute.

Nevertheless, the energy profile of the $DHFR_{tag}$ clearly shows that there is a significant electrostatic barrier, ΔE_{es}^{trans}, to overcome when the body of the DHFR moves through the constriction of the pore (Figure 2b). Moreover, we observed a second smaller electrostatic barrier, ΔE_{es}^{cis}, toward the *cis* side so that an energetic minimum exists inside ClyA in which the molecule can reside. The size difference between these two barriers clearly suggests that in the absence of an external force (*i.e.*, at 0 mV bias) the molecule will exit toward *cis* with overwhelming probability.

To estimate how the charges on DHFR impact its dwell time, we modified the number of charges in the body from −10 to −13 *e* and recomputed the energy landscape using APBS (Figure 2c). We found that the electrostatic energy barrier toward *cis* was largely unaffected (0.04 k_BT increase per negative charge), whereas the barrier for *trans* exit increased significantly (1.46 k_BT increase per negative charge). The latter is a reflection of the highly negatively charged and narrow *trans* constriction of ClyA.

Contrary to the body of DHFR, the modification of the charge in the tag from +4 to +9 *e* influenced the heights of both the *cis* and the *trans* barrier similarly, with increases of 0.621 k_BT and 0.875 k_BT per positive elementary charge, respectively (Figure 2d). This behavior can be explained by the fact that, at DHFR's equilibrium position within the pore, the positively charged tag resides in the highly negatively electrostatic well present in the *trans* constriction of the nanopore (Figure 2b). Moving the molecule from this position into either direction requires this Coulombic attraction to be overcome, which is directly proportional to the number of charges on the tag, irrespective of whether the molecule moves toward *cis* or toward *trans*.

Note that when an external electric field is applied, the electrophoretic and electro-osmotic forces must be taken into account. If their net balance is positive (*i.e.*, a net force toward *cis*) or negative (*i.e.*, a net force toward *trans*), the electrostatic landscape will be tilted upward and downward, respectively (see Figure S3c). The capture of highly negative charged (−11 *e*) wild-type DHFR molecules against the electric field[50] strongly indicates that the electro-osmosis outweighs electrophoresis, and the energy landscape will be shifted downward at *trans*, resulting in higher and lower barrier heights at *cis* and

DOI: 10.1021/acsnano.8b09137
ACS Nano 2019, 13, 9980−9992

Table 1. Mutations and Charges of All DHFR Variants

	mutations[a]		protein charge at pH 7.5 [e]		
name	body (res. 1−163)	tag (res. 164−190)	body	tag	total
$DHFR_4S$			−10	+4	−6
$DHFR_4I$	V88E P89E		−12	+4	−8
$DHFR_4C$	A82E A83E		−12	+4	−8
$DHFR_4O1$	E71Q		−12	+4	−8
$DHFR_4O2$	T68E R71E		−13	+4	−9
$DHFR_5O1$	E71Q	A175K	−12	+5	−7
$DHFR_7O1$	E71Q	A175K A174K A176K	−12	+7	−5
$DHFR_5O2$	T68E R71E	A175K	−13	+5	−8
$DHFR_6O2$	T68E R71E	A175K A174K	−13	+6	−7
$DHFR_7O2$	T68E R71E	A175K A174K A176K	−13	+7	−6
$DHFR_8O2$	T68E R71E	A175K A174K A176K A169K	−13	+8	−5
$DHFR_9O2$	T68E R71E	A175K A174K A176K A169K L177K	−13	+9	−4

[a]With respect to $DHFR_4S$.

trans, respectively. This effectively deepens the energy minimum, which should manifest as an increase of DHFR's dwell time.

Dwell Time Measurements. The entry of a single protein into ClyA results in a temporary reduction of the ionic current from the "open pore" (I_0) to a characteristic "blocked pore" (I_b) level. Previously, we revealed that the DHFR protein shows a main current blockade with $I_{res}\% = I_b/I_0 \approx 70\%$ (see Figure S4). However, occasionally deeper blocks are observed, which most likely represent the transient visit of DHFR to multiple locations inside the nanopore. Here, we assume that the dwell time (t_d) is simply given by the time from the initial capture to the final release where the current level returns to the open-pore current.

After gathering sufficient statistics for the dwell time events, we computed the expectation value of t_d by taking the arithmetic mean of all dwell time events. This is because the chance for an escape can be modeled as the probability of overcoming a potential barrier whose distribution function is exponential (see Supporting Information section 1). Note that even if the molecule transitions through multiple meta-states with individual rates connecting each of them before it exits, the expectation value is still given by the arithmetic mean (see Supporting Information eq S12).

We observed before that the dwell time of tagged DHFR molecules depends strongly on the applied bias,[55] that is, exponentially rising with voltage until a certain bias—which we will refer to as the *threshold voltage*—followed by an exponential fall. This behavior has also been observed for charged peptides in α-hemolysin[44] and is typical for a decay of a bound state into multiple final states, such as an escape to either *cis* or *trans* (see Supporting Information section 1). Therefore, the dwell time of the molecule, as a function of bias voltage, V^{bias}, can be expressed as the inverse of the sum of two escape rates:[44]

$$\frac{1}{t_d} = k = k^{cis} + k^{trans} = k_0^{cis} e^{-\alpha^{cis} eV^{bias}/k_B T} + k_0^{trans} e^{\alpha^{trans} eV^{bias}/k_B T} \quad (1)$$

where $k^{cis/trans}$ are the molecule's escape rates toward *cis* and *trans*, respectively. These can be further decomposed into attempted frequencies $k_0^{cis/trans}$ and bias-dependent barriers in the exponentials. Although this equation can help to qualitatively describe the experimental data, the reduction of the entire protein−nanopore system to four parameters does not allow for their physical interpretation.

Engineering DHFR's Dwell Time by Manipulation of Its Charge. The results from the APBS simulations, together with the previous work with $DHFR_{tag}$ and MTX,[50] suggest that the dwell time of DHFR in ClyA can be increased by the manipulation of its charge distribution. To achieve the increase in dwell time without the need for MTX, several nonconserved amino acids on the surface of $DHFR_4S$ were identified and mutated to negatively charged glutamate residues, resulting in the molecules $DHFR_4I$, $DHFR_4C$, $DHFR_4O1$, and $DHFR_4O2$ (Table 1 and Figure 3a). These mutations modify the number of charges in the body compared to $DHFR_4S$, and their charges are also in different locations. For convenience, this series of mutations will be referred to as the *body charge variations* from here on out.

We performed ionic current measurements for all body charge variations for a wide range of bias voltages (−40 to −120 mV; see Figures S4 and S5) and extracted the dwell times as shown in Figure 3b. All body charge variations showed the same increase of the dwell time at low electric fields and decreased at high fields. However, we observed differences in the threshold voltage and the magnitude of the maximum dwell time. These differences cannot simply be explained by the total number of charges as $DHFR_4I$ and $DHFR_4C$ have the same charge as $DHFR_4O1$, but their dwell times are 10-fold lower (Figure 3b). This result implies that the location of the body charge on DHFR plays an important role.

Additional body mutations could potentially compromise the catalytic cycle of DHFR. Hence, we proceeded by systematically increasing the number of positive charges to the fusion tag (N_{tag}) of $DHFR_4O2$, the variant that exhibited the longest dwell time, *via* lysine substitution from 4 e to 9 e (Table 1 and Figure 4). The resulting $DHFR_{N_{tag}}O2$ mutants will be referred to as the *tag charge variations*.

Subsequent characterization of their the dwell times revealed that the addition of positive charges to the tag significantly increased DHFR's dwell time (Figure 4b). We observed a similar increase for $DHFR_4O1$ variants with +5 and +7 tag charge numbers (see Figure S7). This behavior is consistent with the tag being trapped electrostatically inside the negatively charged *trans* constriction,[44,46,47,60] and it suggests that the tag

DOI: 10.1021/acsnano.8b09137
ACS Nano 2019, 13, 9980−9992

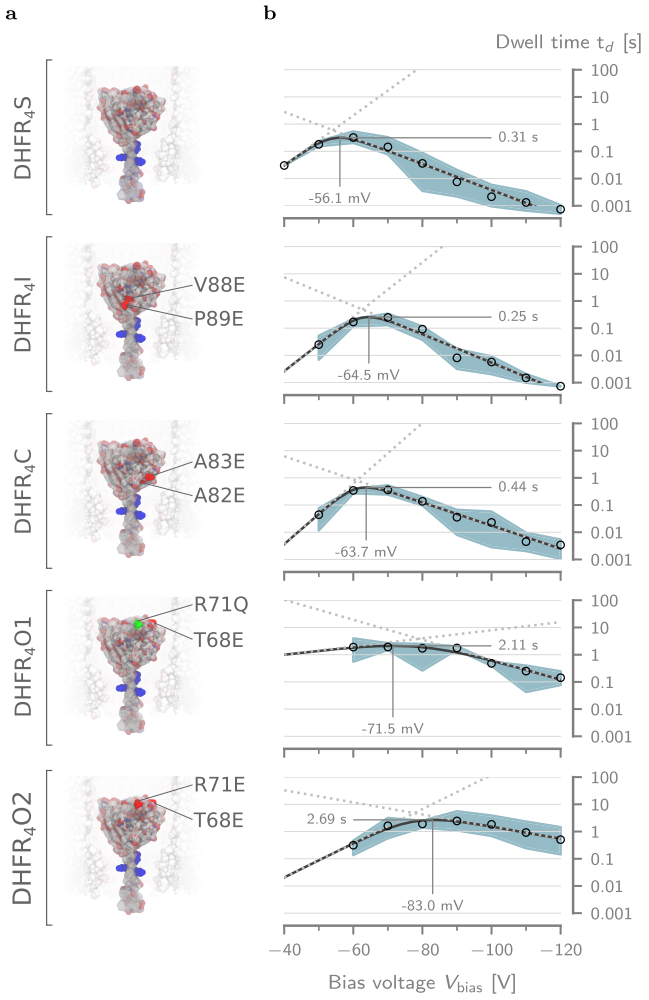

Figure 3. Effect of the body charge on the dwell time of tagged DHFR. (a) Surface representation of the five tested DHFR$_4$X body charge mutants. The mutated residues are indicated for each variant. The positive charges in the fusion tag are colored blue. From top to bottom: DHFR$_4$S, DHFR$_4$I, DHFR$_4$C, DHFR$_4$O1, and DHFR$_4$O2. (b) Voltage dependence of the average dwell time (t_d) inside ClyA-AS for DHFR mutants in (a). The solid lines represent the voltage dependency predicted by fitting the double barrier model given by eq 1 to the data (see Table S4). The dotted lines represent the dwell times due the *cis* (low to high) and *trans* (high to low) barriers. The threshold voltages at the maximum dwell time were estimated by inserting the fitting parameters into eq S25. The error envelope represents the minimum and maximum values obtained from repeats at the same condition. All measurements were performed at ≈28 °C in aqueous buffer at pH 7.5 containing 150 mM NaCl and 15 mM Tris-HCl. Current traces were sampled at 10 kHz and filtered using a low-pass Bessel filter with a 2 kHz cutoff.

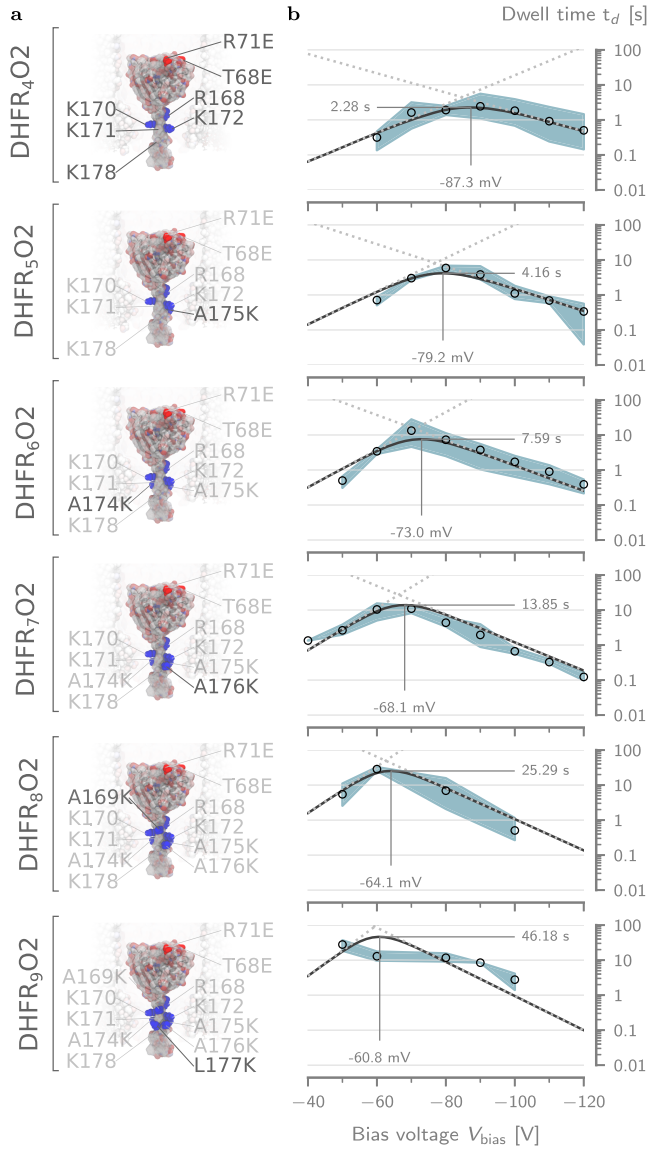

Figure 4. Effect of the tag charge on the dwell time of DHFR$_{N_{tag}}$O2. (a) Surface representations of all DHFR$_{N_{tag}}$O2 mutants going from N_{tag} = 4 (top) to N_{tag} = 9 (bottom). The positively charged residues in the tag have been annotated and highlighted in blue. (b) Voltage dependencies of the mean dwell time (t_d) for the mutant on the left-hand side, fitted with the double barrier model of eq 6. The annotated threshold voltages were computed by Supporting Information eq S26. Solid lines represent the double barrier dwell time, and the dotted lines show the dwell times due the *cis* (low to high) and *trans* (high to low) barriers. Fitting parameters can be found in Table 2. The error envelope represents the minimum and maximum values obtained from repeats at the same condition. Experimental conditions are the same as those in Figure 3.

plays a crucial role in the trapping of DHFR, which was already observed in previous work.[50]

Binding of NADPH Reveals That DHFR Remains Folded Inside the Pore. To verify that our DHFR variants remained folded inside the nanopore, we measured and analyzed the binding of NADPH to the enzyme. The addition of the NADPH cofactor to the *trans* solution of nanopore-entrapped DHFR molecules induced reversible ionic current enhancements that reflect the binding and unbinding of the cofactor to the protein (Figure 5a and Supporting Information Figure S6 and Table S3).

Not all DHFR variants were found to be suitable for NADPH-binding analysis: DHFR$_5$O2 did not dwell long enough inside ClyA-AS at −60 mV (t_d = 0.32 ± 0.17 s) to allow a detailed characterization of NADPH binding, whereas NADPH-binding events to DHFR$_8$O2 were too noisy for a proper determination of k_{on} and k_{off}. No NADPH-binding events to DHFR$_9$O2 could be observed. NADPH-binding events to the other DHFR variants (DHFR$_5$O2, DHFR$_6$O2, and DHFR$_7$O2) showed similar values for k_{on}, k_{off}, and event amplitude (Table S3), suggesting that the binding of NADPH

DOI: 10.1021/acsnano.8b09137
ACS Nano 2019, 13, 9980−9992

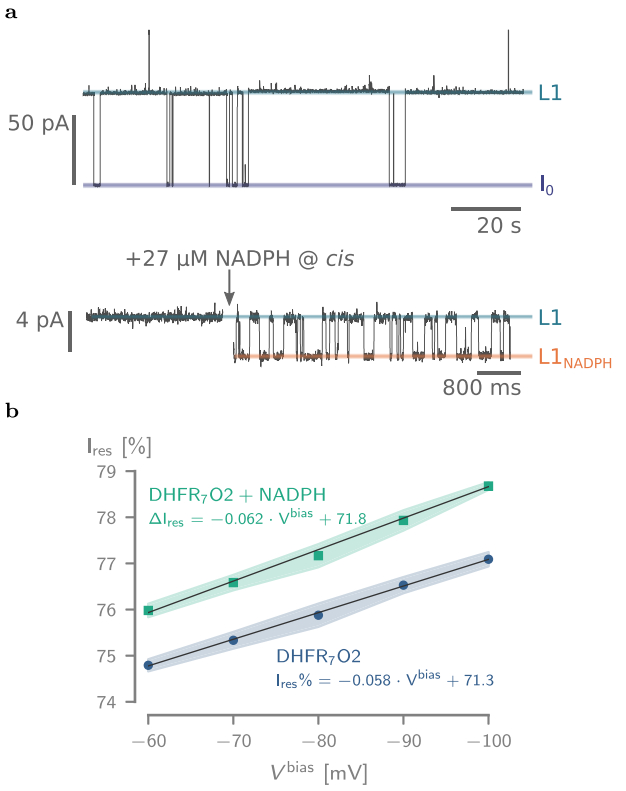

Figure 5. Binding of NADPH to DHFR$_7$O2. (a) Top: Typical current trace after the addition of 50 nM DHFR$_7$O2 to a single ClyA-AS nanopore added to the *cis* reservoir at −60 mV applied potential. The open-pore current (I_0) and the blocked pore levels (L1) are highlighted. Bottom: Current trace showing the blocked pore current of a single DHFR$_7$O2 molecule (50 nM, *cis*) at −60 mV applied potential before (left) and after (right) the addition of 27 μM NADPH to the *trans* compartment. NADPH binding to confined DHFR molecule is reflected by current enhancements from the unbound L1 to the NADPH-bound $L1_{NADPH}$ current levels and showed association (k_{on}) and dissociation (k_{off}) rate constants of 2.03 ± 0.58 × 10^6 M^{-1}·s^{-1} and 71.2 ± 20.4 s^{-1}, respectively (see Table S3). (b) Dependence of the I_{res}% on the applied potential for DHFR$_7$O2 and DHFR$_7$O2 bound to NADPH. All current traces were collected in 250 mM NaCl and 15 mM Tris-HCl, pH 7.5, at 23 °C, by applying a Bessel low-pass filter with a 2 kHz cutoff and sampled at 10 kHz.

to DHFR inside the ClyA-AS nanopore is not affected by the number of positive charges in the C-terminal fusion tag. Possibly, the inability of DHFR$_8$O2 and DHFR$_9$O2 to bind the substrate is due the lodging of DHFR closer to the *trans* constriction.

Work with solid-state nanopores also previously reported that electric fields inside a nanopore may unfold proteins during translocation,[69] suggesting that the high degree of charge separation between the body and tag of DHFR might destabilize its structure. To further investigate the effect of the applied potential on the protein structure, we analyzed the dependency of the residual current on the applied potential (Figure 5). We found that the residual current of both the apo-DHFR and the ligand-bound enzyme increased by ≈2.5% from −60 to −100 mV. A voltage-dependent change in residual current is compatible with a force-induced stretching of the enzyme. However, single-molecule force spectroscopy experiments showed that NADPH binding increases the force required to unfold the protein by more than 3-fold from 27 to 98 pN.[70] As the change of residual current over the potential was identical for both apo- and ligand-bound DHFR (Figure 5), a likely explanation is that, rather than stretching DHFR, the applied bias changes the position of DHFR within the nanopore. Hence, our data suggest that, as previously reported for several other proteins,[52,53] the protein remains folded at different applied bias.

Double Barrier Model for the Trapping of DHFR. Inspired by the strong dependence of the dwell time on the tag charge, we set out to understand the underlying trapping mechanism by building a quantitative model. To this end, we will focus on the data set of the dwell time of DHFR$_{N_{tag}}$O2 shown in Figure 4b.

We propose a double barrier model that describes the trapping of the molecule as a combination of escape rates toward *cis* and toward *trans* (see Supporting Information section 1.3). Similar to eq 1, the dwell time is defined in terms of the rate k, which in turn is given by the sum of the rate for *cis* exit and the rate for *trans* exit. However, now we define the rates in terms of energy barriers:

$$\frac{1}{t_d} = k = k_0 e^{-\Delta E^{cis}/k_B T} + k_0 e^{-\Delta E^{trans}/k_B T} \tag{2}$$

where k_0 is the attempt rate and $\Delta E^{cis/trans}$ are the energy barriers the molecule has to overcome in order to escape toward *cis* and *trans*, respectively. These can be readily decomposed into *steric*, *electrostatic*, and *external* contributions:

$$\Delta E^{cis} = \Delta E^{cis}_{st,0} + \Delta E^{cis}_{es} + \Delta E^{cis}_{ex} \tag{3a}$$

$$\Delta E^{trans} = \Delta E^{trans}_{st,0} + \Delta E^{trans}_{es} + \Delta E^{trans}_{ex} \tag{3b}$$

The steric components $\Delta E^{cis/trans}_{st,0}$ are defined as those interactions of the molecule with the nanopore that are not electrostatic in nature, such as size- or conformation-related effects as DHFR translocates through the narrow constriction toward *trans*.

Supported by the APBS simulations (Figure 2b) and the corresponding barrier height to tag charge dependency analyses (Figure 2d), we infer that the electrostatic components $\Delta E^{cis/trans}_{es}$ can be further decomposed as

$$\Delta E^{cis}_{es} = \Delta E^{cis}_{es,0} + N_{tag} e \Delta V^{cis}_{tag} \tag{4a}$$

$$\Delta E^{trans}_{es} = \Delta E^{trans}_{es,0} + N_{tag} e \Delta V^{trans}_{tag} \tag{4b}$$

where $\Delta V^{cis/trans}_{tag}$ are the electrostatic potentials associated with the tag charge N_{tag} for the *cis* and *trans* barriers (*i.e.*, the change in barrier height per additional charge in N_{tag}) and $\Delta E^{cis/trans}_{es,0}$ are two constant terms that combine all electrostatic interactions between the protein and the pore that do not depend on N_{tag} (*e.g.*, body-charge-related interactions with the electric fields in the nanopore).

The external forces acting on a protein trapped inside ClyA under applied bias voltages manifest in the barrier contribution $\Delta E^{cis/trans}_{ex}$. They comprise an *electrophoretic* component $\Delta E^{cis/trans}_{ep}$ and an *electro-osmotic* component $\Delta E^{cis/trans}_{eo}$. The former results from the strong electric field (≈3.5 × 10^6 V·m^{-1} at −50 mV) and the nonzero net charge on the molecule, whereas the latter springs from the force exerted by ClyA's electro-osmotic flow, which is strong enough to allow the capture of negatively charged proteins even in opposition to the electrophoretic force.[38,49,50,55] If it is assumed that the bias potential changes linearly over the length of the pore, the

DOI: 10.1021/acsnano.8b09137
ACS Nano 2019, 13, 9980−9992

external energy barriers are given by (see Supporting Information section 1)

$$\Delta E_{ex}^{cis} = \Delta E_{ep}^{cis} + \Delta E_{eo}^{cis} = -(N_{net} + N_{eo})e\frac{\Delta x^{cis}}{L}V^{bias} \quad (5a)$$

$$\Delta E_{ex}^{trans} = \Delta E_{ep}^{trans} + \Delta E_{eo}^{trans} = +(N_{net} + N_{eo})e\frac{\Delta x^{trans}}{L}V^{bias} \quad (5b)$$

where $N_{net} = N_{body} + N_{tag}$ is the total number of charges on DHFR, L is the length of the nanopore (14 nm), and V^{bias} is the negative applied bias. The strength of the electro-osmotic force is defined by the *equivalent osmotic charge number* N_{eo}—the number of charges that must be added to DHFR to create an equal electrophoretic force on the molecule. Defining the electro-osmotic force in terms of an equivalent osmotic charge number reveals its complete analogy to an electrophoretic force, which has the benefit that the magnitudes of both forces can be readily compared. Moreover, the equivalent osmotic charge number is an invariant related solely to the size and shape of the molecule.

The quantities $\Delta x^{cis/trans}$ are defined as the distances from the electrostatic energy minimum to the *cis* and *trans* barriers, which depend on the energetic landscape of ClyA and on the precise location of residence of DHFR within the pore. To estimate these values, we can use the APBS simulations (Figure 2b) from which we can read that $\Delta x^{trans} \approx 3.5$ nm. The *cis* distance is more difficult to define as the *cis* electrostatic barrier is much shallower. Without external fields, it has a distance of about ≈2.7 nm, but as we can see in Figure S3c, when the energy landscape is tilted by an external force, the barrier that needs to be overcome is actually located at the *cis* entrance of the pore. In practice, Δx^{cis} will need to be adjusted to a value between these two possibilities to give an adequate estimate and hence will be left as a fitting parameter.

Inserting eqs 3–5 into eq 2 yields the final dwell time model:

$$\frac{1}{t_d} = k = k_{eff}^{cis}\exp\left(-\frac{N_{tag}e\Delta V_{tag}^{cis} - \left(N_{net} + N_{eo}\right)e\frac{\Delta x^{cis}}{L}V^{bias}}{k_BT}\right) + k_{eff}^{trans}\exp\left(-\frac{N_{tag}e\Delta V_{tag}^{trans} + \left(N_{net} + N_{eo}\right)e\frac{\Delta x^{trans}}{L}V^{bias}}{k_BT}\right) \quad (6)$$

where the static terms are absorbed into the prefactor to form the effective *cis* and *trans* barrier attempt rates $k_{eff}^{cis/trans}$. The formulation of eq 6 offers a compact description of the most salient features of the molecule–nanopore system, and it enables us to describe the dwell time of DHFR inside ClyA quantitatively as a function of the physical properties of the system. Fitting this model to all $DHFR_{N_{tag}}O2$ data *simultaneously*—with both V^{bias} and N_{tag} as independent variables—leads to the fitting values in Table 2 and the plots in Figure 4b, which show excellent accuracy considering the simplicity of our model. This is a strong indication that we captured the essence of the trapping mechanism within our model.

Characteristics of the Trapping. As the double barrier model of eq 6 is derived from the underlying physical interactions of the molecule with the nanopore and with the externally applied field, the fitted parameters of Table 2 are physically relevant quantities that describe the characteristics of the system.

Table 2. Fitting Parameters for $DHFR_{N_{tag}}O2$

parameter	description	type	value[a]
V^{bias}	applied bias voltage	independent	40 to 120 mV
N_{tag}	tag charge number	independent	4 to 9
N_{body}	body charge number	fixed	−13
N_{eo}	equivalent osmotic charge number	dependent	15.5 ± 0.9
L	nanopore length	fixed	14 nm
Δx^{trans}	distance to *trans* barrier[b]	fixed	3.5 nm
Δx^{cis}	distance to *cis* barrier[b]	dependent	5.21 ± 1.32 nm
ΔV_{tag}^{trans}	change of ΔE_{es}^{trans} with tag charge	dependent	0.860 ± 0.078 k_BT/e
ΔV_{tag}^{cis}	change of ΔE_{es}^{cis} with tag charge	dependent	0.218 ± 0.167 k_BT/e
$\ln(k_{eff}^{trans}/\mathrm{Hz})$	effective attempt rate for the *trans* barrier	dependent	−3.44 ± 1.24 (3.21×10^{-2} Hz)
$\ln(k_{eff}^{cis}/\mathrm{Hz})$	effective attempt rate for the *cis* barrier	dependent	7.39 ± 1.02 (1.62×10^{3} Hz)

[a]Errors are confidence intervals for one standard deviation. [b]Relative to the energetic minimum inside the pore.

The sizes of the electrostatic barriers $\Delta V_{tag}^{cis/trans}$ that the tag charges experience are in direct relation to the gradients of the barrier sizes computed using the APBS model (Figure 2d). We find that the change of the *trans* barrier with respect to tag charge, $\Delta V_{tag}^{trans} = 0.860\ k_BT$, is in excellent agreement with the simulated gradient of $0.875\ k_BT/e$. The change observed for the *cis* barrier, $\Delta V_{tag}^{cis} = 0.218\ k_BT/e$, is approximately 3-fold smaller compared to its APBS value of $0.621\ k_BT/e$. This deviation likely results from the shallowness of the *cis* barrier, causing it to disappear when the energy landscape is tilted under an applied bias voltage (see Figure S3b). This gives rise to a *cis* barrier that lies at a location further away from the electrostatic minimum located inside the *trans* constriction, effectively limiting the influence of the tag charge number on the barrier height. This claim is further corroborated by the finding that the fitted value of $\Delta x^{cis} \approx 5.2$ nm, which is almost twice the distance predicted by the APBS simulations and moves that *cis* barrier much closer to the *cis* entry.

One of the key insights we obtain from our model is the ability to directly extract information on the strength of the osmotic flow. However, let us first observe that the equivalent electro-osmotic charge number $N_{eo} \approx 15.5$ is much bigger than the net charge of all tag charge variations, $N_{tag} + N_{body} = -9, \ldots, -4$, and also has the opposite sign. This is in agreement with the earlier assumption that the electro-osmotic force is strong enough to overcome the opposing electrophoretic force and is hence responsible for the capture of the molecule.[38,50] At a bias of $V^{bias} = -50$ mV, the electro-osmotic force exerted onto the DHFR molecule, as computed by eq S21, is

$$F_{eo} \approx 9\ \mathrm{pN} \quad (7)$$

The magnitude of this force is in line with those found experimentally for DNA[71−73] and proteins[74] in solid-state nanopores.

DOI: 10.1021/acsnano.8b09137
ACS Nano 2019, 13, 9980−9992

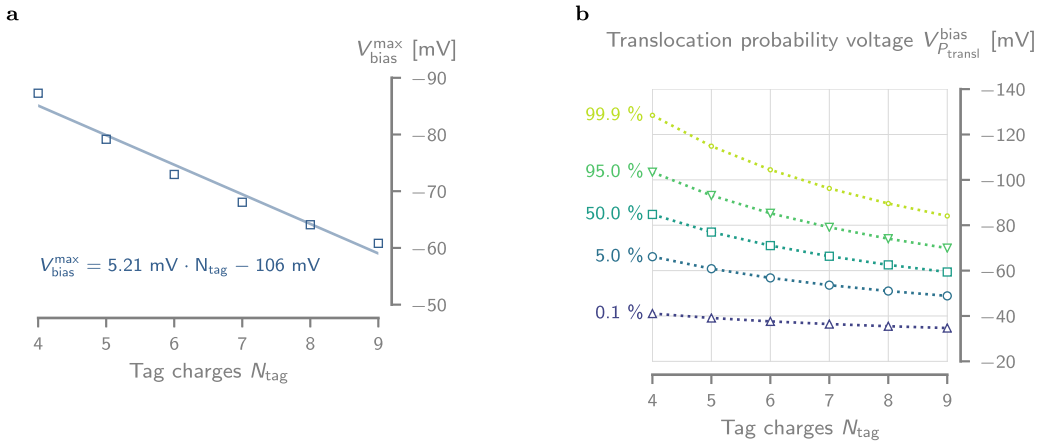

Figure 6. Tag charge dependence of the threshold voltage and translocation probability. (a) Every additional positive charge in the fusion tag of the DHFR$_{N_{tag}}$O2 variants increases the threshold voltage (see Supporting Information S26) by ≈5.21 mV. The solid line is a linear fit to the data. (b) Translocation probability voltage $V_{P_{transl}}^{bias}$ plotted against tag charge for P_{transl} = 0.1, 5, 50, 95 and 99.9% shows that variants with high tag charge require less bias voltage to fully translocate the pore. Values were obtained through interpolation from eq 8, using the parameters in Table 2.

We found the threshold voltages—obtained from the fitted model—to be roughly linearly dependent on the number of tag charges, with a decrease of ≈5 mV per additional positive charge (Figure 6a). This effect is caused by the increase of the net external force on the molecule with increasing tag charge, resulting in a simultaneous lowering of the *trans* barrier and raising the *cis* barrier.

Another important finding of our model is that the DHFR variations are essentially trapped by the electrostatic forces of the pore on the tag. This can be seen from the direct exponential dependence of the electrostatics on the tag charge as shown in eq 4. If the molecule was trapped as a whole between two barriers, we would rather see a dependence on the net charge on the molecule. Indeed, we verified that such a net charge dependence *cannot* be fitted to the data. This suggests that the tag acts as an anchor which is located in the electrostatic minimum created by the *trans* constriction (Figure 2a).

We can also determine the probability of a full translocation of DHFR using

$$P_{transl} = k^{trans}/(k^{cis} + k^{trans}) \quad (8)$$

where k^{cis} and k^{trans} can be computed using the individual components given by eq 6 and the parameters in Table 2. At zero bias and zero tag charge, we find that only 0.002% of DHFR molecules would exit to the *trans* side, indicating that in the absence of an electrophoretic driving force a *cis* exit is much more likely than a *trans* exit. This is in agreement with our expectations because DHFR's size leads to a significant steric hindrance when it tries to translocate through the nanopore constriction.

Finally, from eq 8, we can compute the voltage $V_{P_{transl}}^{bias}$ required to obtain a given translocation probability (Figure 6). The number of tag charges significantly lowers the voltage required to achieve full translocation, for example, $V_{P_{transl}}^{bias}$ for P_{transl} = 99.9 decreases from −130 mV to −85 mV going from N_{tag} = +4 to +9. This effect is mainly due to the lowering of the *trans* barrier height, as the *cis* escape probability voltage (0.01% line in Figure 6) only changes from −40 mV to −35 mV going from +4 to +9 tag charges. Hence, the higher the tag charge number, the stronger the net external force which pushes the molecule through the *trans* constriction of the pore.

CONCLUSIONS

We showed previously that neutral or weakly charged proteins larger than the *trans* constriction (>3.3 nm) of ClyA can be trapped inside the nanopore for a relatively long duration (seconds to minutes) and that their behavior can be sampled by ionic current recordings.[38,49,50,54,55] In contrast, small proteins rapidly translocate through the nanopore due to the strong electro-osmotic flow, and highly negatively charged proteins remain inside ClyA only briefly or they do not enter at all.[38]

In this work, we use DHFR as a model molecule to enhance and investigate the trapping of small and negatively charged proteins inside the ClyA nanopore.[55] DHFR (3.5−4 nm) is slightly too large to pass through the *trans* constriction, and its negatively charged body (N_{body} = −13 *e*) only allowed trapping the protein inside the nanopore for a few milliseconds. The introduction of a positively charged C-terminal fusion tag partially counterbalanced the electrophoretic force and introduced an electrostatic trap in the *trans* constriction of ClyA that increased the DHFR dwell time up to minutes.

The DHFR mutants showed a biphasic voltage dependency which was explained by using a physical model containing a double energy barrier to account for the exit on either side of the nanopore. The model contained steric, electrostatic, electrophoretic, and electro-osmotic components, and it allowed us to describe the complex voltage-dependent data for the different DHFR constructs. Furthermore, fitting to experimental data of a series of DHFR$_{N_{tag}}$O2 constructs, in which the positive charge of the tag was systematically increased, enabled us to deduce meaningful values for DHFR's intrinsic *cis* and *trans* translocation probabilities as well as an estimate of the force exerted by the electro-osmotic flow on the protein of 0.178 pN·mV^{-1} (*e.g.*, 9 pN at −50 mV, Table 2). We also showed that the APBS simulation results of a simple bead model for the molecule are directly related to the independently fitted parameters of the double barrier model. In conclusion, this means that it should be possible to *predict* the

DOI: 10.1021/acsnano.8b09137
ACS Nano 2019, 13, 9980−9992

dwell times of similar experiments by obtaining parameters directly from these types of APBS simulations.

The double barrier model of eq 6 in its current form does not adequately describe the mutations that modify the body charge distribution of DHFR. This is most likely because body charge variations close to the electrostatically trapped tag will impact the height of the barriers more strongly than modifications on the far end of the tag. Although a model accounting for this effect could be made, it would also make the double barrier model significantly more complex without providing any significant advantages over a more comprehensive atomistic simulation. A more detailed discussion can be found in the Supporting Information section 4.

Inside the lumen of ClyA, proteins are able to bind to their specific substrates at all applied potentials tested (up to −100 mV), indicating that the electrostatic potential inside the nanopore and the electrostatic potential originating from the inner surface of the nanopore did not unfold the protein. Therefore, our results indicate that ClyA nanopores can be used as nanoscale test tubes to investigate enzyme function at the single-molecule level. Compared to the wide variety of single-molecule techniques based on fluorescence, nanopore recordings are label-free, which have the advantage of allowing long observation times.

The electrophoretic trapping of proteins inside nanopores is likely to have practical applications. For example, arrays of biological or solid-state nanopores will allow the precise alignment of proteins on a surface. In addition, proteins immobilized inside glass nanopipettes atop a scanning ion conductance microscope[75,76] can be manipulated with nanometer-scale precision, which might be used, for instance, for the localized delivery of proteins. Furthermore, ionic current measurements through the nanopore can be used for the detection of analyte binding to an immobilized protein, which has applications in single-molecule protein studies and small analyte sensing.

MATERIALS AND METHODS

Electrostatic Energy Landscape Computation. The electrostatic energy landscape of a coarse-grained DHFR molecule translocating through a full-atom ClyA model was computed using the adaptive Poisson−Boltzmann solver (APBS).[61] The full procedure is described in the Supporting Information section 2. In summary, a full atom model of ClyA-AS[60] was prepared *via* homology modeling with the MODELLER software package[57] from the wild-type ClyA crystal structure (PDB ID: 2WCD[56]), and its energy was further minimized using the VMD[58] and NAMD programs.[59] A coarse-grained bead model of DHFR—consisting of a "body" of seven negatively charged beads in a spherical configuration and a "tail" of nine smaller beads in a linear configuration with varying charge—was placed a various locations along the central axis of the pore using custom Python code and the Biopython package.[77] Each atom in the resulting ClyA−DHFR complexes was subsequently assigned a radius and partial charge (according to the CHARMM36 force-field[78]) with the PDB2PQR program,[62,63] and the electrostatic energy was computed with APBS. The net electrostatic energy cost or gain of placing a DHFR molecule at a given location inside ClyA ($\Delta G^{\text{pore+part}}$) is then given by

$$\Delta G^{\text{pore+part}} = G^{\text{pore+part}} - G^{\text{pore}} - G^{\text{part}} \quad (9)$$

with $G^{\text{pore+part}}$, G^{pore}, and G^{part} being the total electrostatic energies of the ClyA−DHFR complex, the empty ClyA pore, and only the DHFR molecule, respectively.

Protein Mutagenesis, Overexpression, and Purification. All DHFR variants were constructed, overexpressed, and purified using standard molecular biology techniques,[50,55] as described in full detail in the Supporting Information section 5.2. Briefly, the $DHFR_4S$ DNA construct was built from the pT7-SC1 plasmid containing the DHFR-tag construct[50] by inserting an additional alanine residue at position 175 (located in the fusion tag) with site-directed mutagenesis. All other variants were derived—again using site-directed mutagenesis—either directly from $DHFR_4S$ or from a variant thereof. The plasmids of each DHFR variant were used to transform E. cloni EXPRESS BL21(DE3) cells (Lucigen, Middleton, USA), and the DHFR proteins they encode were overexpressed overnight at 25 °C in a liquid culture. After the bacterial cells were harvested by centrifugation, the overexpressed proteins were released into solution through lysis—using a combination of at least a single freeze−thaw cycle, incubation with lysozyme, and probe−tip sonification. Finally, the DHFR proteins were purified from the lysate with affinity chromotography with Strep-Tactin Sepharose (IBA Lifesciences, Goettingen, Germany), aliquoted, and stored at −20 °C until further use.

ClyA-AS Overexpression, Purification, and Oligomerization. ClyA-AS oligomers were prepared as described previously,[49] and full details can be found in the Supporting Information section 5.2. Briefly, the ClyA-AS monomers were overexpressed and purified in a manner similar to that for DHFR, with the largest difference being the use of Ni-NTA-based affinity chromotography. After purification, ClyA-AS monomers were oligomerized in 0.5% β-dodecylmaltoside (GLYCON Biochemicals GmbH, Luckenwalde, Germany) at 37 °C for 30 min. The type I oligomer (12-mer) was isolated by gel extraction from a blue native PAGE.

Electrical Recordings in Planar Lipid Bilayers. Electrical recordings of individual ClyA-AS nanopores were carried out using a typical planar lipid bilayer setup with an AxoPatch 200B (Axon Instruments, San Jose, USA) patch-clamp amplifier.[38,79] Briefly, a black lipid membrane consisting of 1,2-diphytanoyl-*sn*-glycero-3-phosphocholine (Avanti Polar Lipids, Alabaster, USA) was formed inside a ≈100 μm diameter aperture in a thin polytetrafluoroethylene film (Goodfellow Cambridge Limited, Huntingdon, England), separating two electrolyte compartments. Single nanopores were then made to insert into the *cis* side chamber (grounded) by addition of 0.01−0.1 ng of preoligomerized ClyA-AS to the buffered electrolyte (150 mM NaCl, 15 mM Tris-HCl, pH 7.5). All ionic currents were sampled at 10 kHz and filtered with a 2 kHz low-pass Bessel filter. A more detailed description can be found in the Supporting Information section 5.4.

Dwell Time Analysis and Model Fitting. The dwell times of the DHFR protein blocks were extracted from single-nanopore channel recordings using the "single-channel search" algorithm of the pCLAMP 10.5 (Molecular Devices, San Jose, USA) software suite. The process was monitored manually, and any events shorter than 1 ms were discarded. We processed the dwell time data and fitted the double barrier model to it, using a custom Python code employing the NumPy,[80] pandas,[81] and lmfit[82] packages. More details can be found in the Supporting Information sections 5.4 and 5.5.

ASSOCIATED CONTENT

Supporting Information

The Supporting Information is available free of charge on the ACS Publications website at DOI: 10.1021/acsnano.8b09137.

Supplementary text and figures for the full derivation of the double barrier model, details of the APBS simulations, examples of raw current traces of all variants, the on- and off-rates of NADPH binding to DHFR, and all materials and methods (PDF)

AUTHOR INFORMATION

Corresponding Author

*E-mail: g.maglia@rug.nl.

DOI: 10.1021/acsnano.8b09137
ACS Nano 2019, 13, 9980−9992

ORCID

Kherim Willems: 0000-0003-1341-1581
Giovanni Maglia: 0000-0003-2784-0811

Author Contributions

[⊥]K.W., D.R., and A.B. contributed equally to this work.

Notes

The authors declare no competing financial interest.

ACKNOWLEDGMENTS

We thank the European Research Council (European Commission's Seventh Framework Programme, Project No. 260884) and the Fund for Scientific Research (FWO, research Project No. G068315N) for funding. A.B. and K.W. were funded by a Ph.D. grant from the Agency for Innovation by Science and Technology (IWT) Flanders. The computational resources and services used in this work were provided by the VSC (Flemish Supercomputer Center), funded by the Research Foundation—Flanders (FWO) and the Flemish Government, department EWI.

REFERENCES

(1) Gooding, J. J.; Gaus, K. Single-Molecule Sensors: Challenges and Opportunities for Quantita- tive Analysis. *Angew. Chem., Int. Ed.* **2016**, *55*, 11354−11366.

(2) Xie, S. Single-Molecule Approach to Enzymology. *Single Mol.* **2001**, *2*, 229−236.

(3) Willems, K.; Van Meervelt, V.; Wloka, C.; Maglia, G. Single-Molecule Nanopore Enzymology. *Philos. Trans. R. Soc., B* **2017**, *372*, 20160230.

(4) Krishnan, M.; Mojarad, N.; Kukura, P.; Sandoghdar, V. Geometry-Induced Electrostatic Trap- ping of Nanometric Objects in a Fluid. *Nature* **2010**, *467*, 692−695.

(5) Myers, C. J.; Celebrano, M.; Krishnan, M. Information Storage and Retrieval in a Single Levitating Colloidal Particle. *Nat. Nanotechnol.* **2015**, *10*, 886−891.

(6) Neuman, K. C.; Block, S. M. Optical Trapping. *Rev. Sci. Instrum.* **2004**, *75*, 2787−2809.

(7) Baker, J. E.; Badman, R. P.; Wang, M. D. Nanophotonic Trapping: Precise Manipulation and Measurement of Biomolecular Arrays. *Wiley Interdiscip. Rev.: Nanomed. Nanobiotechnol.* **2018**, *10*, No. e1477.

(8) Bradac, C. Nanoscale Optical Trapping: A Review. *Adv. Opt. Mater.* **2018**, *6*, 1800005.

(9) Yang, A. H. J.; Moore, S. D.; Schmidt, B. S.; Klug, M.; Lipson, M.; Erickson, D. Optical Manipulation of Nanoparticles and Biomolecules in Sub-Wavelength Slot Waveguides. *Nature* **2009**, *457*, 71−75.

(10) Mandal, S.; Serey, X.; Erickson, D. Nanomanipulation Using Silicon Photonic Crystal Res- onators. *Nano Lett.* **2010**, *10*, 99−104.

(11) Juan, M. L.; Gordon, R.; Pang, Y.; Eftekhari, F.; Quidant, R. Self-induced back-action optical trapping of dielectric nanoparticles. *Nat. Phys.* **2009**, *5*, 915−919.

(12) Chen, C.; Juan, M. L.; Li, Y.; Maes, G.; Borghs, G.; Van Dorpe, P.; Quidant, R. Enhanced Optical Trapping and Arrangement of Nano-Objects in a Plasmonic Nanocavity. *Nano Lett.* **2012**, *12*, 125−132.

(13) Pang, Y.; Gordon, R. Optical Trapping of a Single Protein. *Nano Lett.* **2012**, *12*, 402−406.

(14) Bergeron, J.; Zehtabi-Oskuie, A.; Ghaffari, S.; Pang, Y.; Gordon, R. Optical Trapping of Nanoparticles. *J. Visualized Exp.* **2013**, DOI: 10.3791/4424.

(15) Kotnala, A.; Al-Balushi, A. A.; Gordon, R. Optical Tweezers for Free-Solution Label-Free Single Bio-Molecule Studies. *Proc SPIE* **2014**, 916418.

(16) Kerman, S.; Chen, C.; Li, Y.; Van Roy, W.; Lagae, L.; Van Dorpe, P. Raman Fingerprinting of Single Dielectric Nanoparticles in Plasmonic Nanopores. *Nanoscale* **2015**, *7*, 18612−18618.

(17) Chen, C.; Li, Y.; Kerman, S.; Neutens, P.; Willems, K.; Cornelissen, S.; Lagae, L.; Stakenborg, T.; Van Dorpe, P. High Spatial Resolution Nanoslit SERS for Single-Molecule Nucleobase Sensing. *Nat. Commun.* **2018**, *9*, 1733.

(18) Verschueren, D.; Shi, X.; Dekker, C. Nano-Optical Tweezing of Single Proteins in Plasmonic Nanopores. *Small Methods* **2019**, *3*, 1800465.

(19) Cohen, A. E.; Moerner, W. E. Method for Trapping and Manipulating Nanoscale Objects in Solution. *Appl. Phys. Lett.* **2005**, *86*, No. 093109.

(20) Cohen, A. E.; Moerner, W. E. Suppressing Brownian Motion of Individual Biomolecules in Solution. *Proc. Natl. Acad. Sci. U. S. A.* **2006**, *103*, 4362−4365.

(21) Goldsmith, R. H.; Moerner, W. E. Watching Conformational- and Photodynamics of Single Fluorescent Proteins in Solution. *Nat. Chem.* **2010**, *2*, 179−186.

(22) Goldsmith, R. H.; Tabares, L. C.; Kostrz, D.; Dennison, C.; Aartsma, T. J.; Canters, G. W.; Moerner, W. E. Redox Cycling and Kinetic Analysis of Single Molecules of Solution-Phase Nitrite Reductase. *Proc. Natl. Acad. Sci. U. S. A.* **2011**, *108*, 17269−17274.

(23) Fields, A. P.; Cohen, A. E. Electrokinetic Trapping at the One Nanometer Limit. *Proc. Natl. Acad. Sci. U. S. A.* **2011**, *108*, 8937−8942.

(24) Ma, L.; Cockroft, S. L. Biological Nanopores for Single-Molecule Biophysics. *ChemBioChem* **2010**, *11*, 25−34.

(25) Laszlo, A. H.; Derrington, I. M.; Gundlach, J. H. MspA Nanopore As a Single-Molecule Tool: From Sequencing to SPRNT. *Methods* **2016**, *105*, 75−89.

(26) Varongchayakul, N.; Song, J.; Meller, A.; Grinstaff, M. W. Single-Molecule Protein Sensing in a Nanopore: a Tutorial. *Chem. Soc. Rev.* **2018**, *47*, 8512−8524.

(27) Fologea, D.; Ledden, B.; McNabb, D. S.; Li, J. Electrical Characterization of Protein Molecules by a Solid-State Nanopore. *Appl. Phys. Lett.* **2007**, *91*, No. 053901.

(28) Plesa, C.; Kowalczyk, S. W.; Zinsmeester, R.; Grosberg, A. Y.; Rabin, Y.; Dekker, C. Fast Translocation of Proteins Through Solid State Nanopores. *Nano Lett.* **2013**, *13*, 658−663.

(29) Li, W.; Bell, N. A. W.; Herńandez-Ainsa, S.; Thacker, V. V.; Thackray, A. M.; Bujdoso, R.; Keyser, U. F. Single Protein Molecule Detection by Glass Nanopores. *ACS Nano* **2013**, *7*, 4129−4134.

(30) Larkin, J.; Henley, R. Y.; Muthukumar, M.; Rosenstein, J. K.; Wanunu, M. High-Bandwidth Protein Analysis Using Solid-State Nanopores. *Biophys. J.* **2014**, *106*, 696−704.

(31) Waduge, P.; Hu, R.; Bandarkar, P.; Yamazaki, H.; Cressiot, B.; Zhao, Q.; Whitford, P. C.; Wanunu, M. Nanopore-Based Measure- ments of Protein Size, Fluctuations, and Conformational Changes. *ACS Nano* **2017**, *11*, 5706−5716.

(32) Hu, R.; Rodrigues, J. V.; Waduge, P.; Yamazaki, H.; Cressiot, B.; Chishti, Y.; Makowski, L.; Yu, D.; Shakhnovich, E.; Zhao, Q.; Wanunu, M. Differential Enzyme Flexibility Probed Using Solid-State Nanopores. *ACS Nano* **2018**, *12*, 4494−4502.

(33) Houghtaling, J.; Ying, C.; Eggenberger, O. M.; Fennouri, A.; Nandivada, S.; Acharjee, M.; Li, J.; Hall, A. R.; Mayer, M. Estimation of Shape, Volume, and Dipole Moment of Individual Proteins Freely Transiting a Synthetic Nanopore. *ACS Nano* **2019**, *13*, 5231.

(34) Wei, R.; Gatterdam, V.; Wieneke, R.; Tampe, R.; Rant, U. Stochastic Sensing of Proteins with Receptor-Modified Solid-State Nanopores. *Nat. Nanotechnol.* **2012**, *7*, 257−263.

(35) Yusko, E. C.; Johnson, J. M.; Majd, S.; Prangkio, P.; Rollings, R. C.; Li, J.; Yang, J.; Mayer, M. Controlling Protein Translocation Through Nanopores with Bio-Inspired Fluid Walls. *Nat. Nanotechnol.* **2011**, *6*, 253−260.

(36) Yusko, E. C.; Bruhn, B. R.; Eggenberger, O. M.; Houghtaling, J.; Rollings, R. C.; Walsh, N. C.; Nandivada, S.; Pindrus, M.; Hall, A. R.; Sept, D.; Li, J.; Kalonia, D. S.; Mayer, M. Real-Time Shape

DOI: 10.1021/acsnano.8b09137
ACS Nano 2019, 13, 9980−9992

Approximation and Fingerprinting of Single Proteins Using a Nanopore. *Nat. Nanotechnol.* **2017**, *12*, 360−367.
(37) Rotem, D.; Jayasinghe, L.; Salichou, M.; Bayley, H. Protein Detection by Nanopores Equipped with Aptamers. *J. Am. Chem. Soc.* **2012**, *134*, 2781−2787.
(38) Soskine, M.; Biesemans, A.; Moeyaert, B.; Cheley, S.; Bayley, H.; Maglia, G. An Engineered ClyA Nanopore Detects Folded Target Proteins by Selective External Association and Pore Entry. *Nano Lett.* **2012**, *12*, 4895−4900.
(39) Lieberman, K. R.; Cherf, G. M.; Doody, M. J.; Olasagasti, F.; Kolodji, Y.; Akeson, M. Processive Replication of Single DNA Molecules in a Nanopore Catalyzed by Phi29 DNA Polymerase. *J. Am. Chem. Soc.* **2010**, *132*, 17961−17972.
(40) Derrington, I. M.; Craig, J. M.; Stava, E.; Laszlo, A. H.; Ross, B. C.; Brinkerhoff, H.; Nova, I. C.; Doering, K.; Tickman, B. I.; Ronaghi, M.; Mandell, J. G.; Gunderson, K. L.; Gundlach, J. H. Subangstrom Single-Molecule Measurements of Motor Proteins Using a Nanopore. *Nat. Biotechnol.* **2015**, *33*, 1073−1075.
(41) Squires, A.; Atas, E.; Meller, A. Nanopore Sensing of Individual Transcription Factors Bound to DNA. *Sci. Rep.* **2015**, *5*, 11643.
(42) Yang, W.; Restrepo-Perez, L.; Bengtson, M.; Heerema, S. J.; Birnie, A.; van der Torre, J.; Dekker, C. Detection of CRISPR-dCas9 on DNA with Solid-State Nanopores. *Nano Lett.* **2018**, *18*, 6469−6474.
(43) Muthukumar, M. Communication: Charge, Diffusion, and Mobility of Proteins Through Nanopores. *J. Chem. Phys.* **2014**, *141*, No. 081104.
(44) Movileanu, L.; Schmittschmitt, J. P.; Scholtz, J. M.; Bayley, H. Interactions of Peptides with a Protein Pore. *Biophys. J.* **2005**, *89*, 1030−1045.
(45) Mereuta, L.; Roy, M.; Asandei, A.; Lee, J. K.; Park, Y.; Andricioaei, I.; Luchian, T. Slowing Down Single-Molecule Trafficking Through a Protein Nanopore Reveals Intermediates for Peptide Translocation. *Sci. Rep.* **2015**, *4*, 03885.
(46) Asandei, A.; Schiopu, I.; Chinappi, M.; Seo, C. H.; Park, Y.; Luchian, T. Electroosmotic Trap Against the Electrophoretic Force Near a Protein Nanopore Reveals Peptide Dynamics During Capture and Translocation. *ACS Appl. Mater. Interfaces* **2016**, *8*, 13166−13179.
(47) Asandei, A.; Chinappi, M.; Lee, J.-k.; Ho Seo, C.; Mereuta, L.; Park, Y.; Luchian, T. Placement of Oppositely Charged Aminoacids at a Polypeptide Termini Determines the Voltage-Controlled Braking of Polymer Transport Through Nanometer-Scale Pores. *Sci. Rep.* **2015**, *5*, 10419.
(48) Mohammad; Prakash, S.; Matouschek, A.; Movileanu, L. Controlling a Single Protein in a Nanopore Through Electrostatic Traps. *J. Am. Chem. Soc.* **2008**, *130*, 4081−4088.
(49) Soskine, M.; Biesemans, A.; De Maeyer, M.; Maglia, G. Tuning the Size and Properties of ClyA Nanopores Assisted by Directed Evolution. *J. Am. Chem. Soc.* **2013**, *135*, 13456−13463.
(50) Soskine, M.; Biesemans, A.; Maglia, G. Single-Molecule Analyte Recognition with ClyA Nanopores Equipped with Internal Protein Adaptors. *J. Am. Chem. Soc.* **2015**, *137*, 5793−5797.
(51) Wloka, C.; Van Meervelt, V.; van Gelder, D.; Danda, N.; Jager, N.; Williams, C. P.; Maglia, G. Label-Free and Real-Time Detection of Protein Ubiquitination with a Biological Nanopore. *ACS Nano* **2017**, *11*, 4387−4394.
(52) Van Meervelt, V.; Soskine, M.; Singh, S.; Schuurman-Wolters, G. K.; Wijma, H. J.; Poolman, B.; Maglia, G. Real-Time Conformational Changes and Controlled Orientation of Native Proteins Inside a Protein Nanoreactor. *J. Am. Chem. Soc.* **2017**, *139*, 18640−18646.
(53) Galenkamp, N. S.; Soskine, M.; Hermans, J.; Wloka, C.; Maglia, G. Direct Electrical Quantification of Glucose and Asparagine from Bodily Fluids Using Nanopores. *Nat. Commun.* **2018**, *9*, 4085.
(54) Van Meervelt, V.; Soskine, M.; Maglia, G. Detection of Two Isomeric Binding Configurations in a Protein−Aptamer Complex with a Biological Nanopore. *ACS Nano* **2014**, *8*, 12826−12835.
(55) Biesemans, A.; Soskine, M.; Maglia, G. A Protein Rotaxane Controls the Translocation of Proteins Across a ClyA Nanopore. *Nano Lett.* **2015**, *15*, 6076−6081.
(56) Mueller, M.; Grauschopf, U.; Maier, T.; Glockshuber, R.; Ban, N. The Structure of a Cytolytic α-Helical Toxin Pore Reveals Its Assembly Mechanism. *Nature* **2009**, *459*, 726−730.
(57) Šali, A.; Blundell, T. L. Comparative Protein Modelling by Satisfaction of Spatial Restraints. *J. Mol. Biol.* **1993**, *234*, 779−815.
(58) Humphrey, W.; Dalke, A.; Schulten, K. VMD: Visual Molecular Dynamics. *J. Mol. Graphics* **1996**, *14*, 33−38.
(59) Phillips, J. C.; Braun, R.; Wang, W.; Gumbart, J.; Tajkhorshid, E.; Villa, E.; Chipot, C.; Skeel, R. D.; Kale, L.; Schulten, K. Scalable Molecular Dynamics with NAMD. *J. Comput. Chem.* **2005**, *26*, 1781−802.
(60) Franceschini, L.; Brouns, T.; Willems, K.; Carlon, E.; Maglia, G. DNA Translocation Through Nanopores at Physiological Ionic Strengths Requires Precise Nanoscale Engineering. *ACS Nano* **2016**, *10*, 8394−8402.
(61) Baker, N. A.; Sept, D.; Joseph, S.; Holst, M. J.; McCammon, J. A. Electrostatics of Nanosystems: Application to Microtubules and the Ribosome. *Proc. Natl. Acad. Sci. U. S. A.* **2001**, *98*, 10037.
(62) Dolinsky, T. J.; Nielsen, J. E.; McCammon, J. A.; Baker, N. A. PDB2PQR: an Automated Pipeline for the Setup of Poisson-Boltzmann Electrostatics Calculations. *Nucleic Acids Res.* **2004**, *32*, W665−W667.
(63) Dolinsky, T. J.; Czodrowski, P.; Li, H.; Nielsen, J. E.; Jensen, J. H.; Klebe, G.; Baker, N. A. PDB2PQR: Expanding and Upgrading Automated Preparation of Biomolecular Structures for Molecular Simulations. *Nucleic Acids Res.* **2007**, *35*, W522−W525.
(64) Thevenet, P.; Shen, Y.; Maupetit, J.; Guyon, F.; Derreumaux, P.; Tuffery, P. PEP-FOLD: an Updated *de novo* Structure Prediction Server for Both Linear and Disulfide Bonded Cyclic Peptides. *Nucleic Acids Res.* **2012**, *40*, W288−W293.
(65) Shen, Y.; Maupetit, J.; Derreumaux, P.; Tuffery, P. Improved PEP-FOLD Approach for Peptide and Miniprotein Structure Prediction. *J. Chem. Theory Comput.* **2014**, *10*, 4745−4758.
(66) Stone, J. An Efficient Library for Parallel Ray Tracing and Animation. M.Sc. Thesis, Computer Science Department, University of Missouri-Rolla, 1998.
(67) Kohen, A. Dihydrofolate Reductase As a Model for Studies of Enzyme Dynamics and Catalysis. *F1000Research* **2015**, *4*, 1464.
(68) Li, H.; Robertson, A. D.; Jensen, J. H. Very Fast Empirical Prediction and Rationalization of Protein pKa Values. *Proteins: Struct., Funct., Genet.* **2005**, *61*, 704−721.
(69) Talaga, D. S.; Li, J. Single-Molecule Protein Unfolding in Solid State Nanopores. *J. Am. Chem. Soc.* **2009**, *131*, 9287−9297.
(70) Ainavarapu, S. R. K.; Li, L.; Badilla, C. L.; Fernandez, J. M. Ligand Binding Modulates the Mechanical Stability of Dihydrofolate Reductase. *Biophys. J.* **2005**, *89*, 3337−3344.
(71) Keyser, U. F.; Koeleman, B. N.; van Dorp, S.; Krapf, D.; Smeets, R. M. M.; Lemay, S. G.; Dekker, N. H.; Dekker, C. Direct Force Measurements on DNA in a Solid-State Nanopore. *Nat. Phys.* **2006**, *2*, 473−477.
(72) van Dorp, S.; Keyser, U. F.; Dekker, N. H.; Dekker, C.; Lemay, S. G. Origin of the Electrophoretic Force on DNA in Solid-State Nanopores. *Nat. Phys.* **2009**, *5*, 347−351.
(73) Lu, B.; Hoogerheide, D. P.; Zhao, Q.; Yu, D. Effective Driving Force Applied on DNA Inside a Solid-State Nanopore. *Phys. Rev. E* **2012**, *86*, 011921.
(74) Oukhaled, A.; Cressiot, B.; Bacri, L.; Pastoriza-Gallego, M.; Betton, J.-M.; Bourhis, E.; Jede, R.; Gierak, J.; Auvray, L.; Pelta, J. Dynamics of Completely Unfolded and Native Proteins through Solid-State Nanopores as a Function of Electric Driving Force. *ACS Nano* **2011**, *5*, 3628−3638.
(75) Bruckbauer, A.; James, P.; Zhou, D.; Yoon, J. W.; Excell, D.; Korchev, Y.; Jones, R.; Klenerman, D. Nanopipette Delivery of Individual Molecules to Cellular Compartments for Single-Molecule Fluorescence Tracking. *Biophys. J.* **2007**, *93*, 3120−3131.

DOI: 10.1021/acsnano.8b09137
ACS Nano 2019, 13, 9980−9992

(76) Babakinejad, B.; Jonsson, P.; Lopez Cordoba, A.; Actis, P.; Novak, P.; Takahashi, Y.; Shevchuk, A.; Anand, U.; Anand, P.; Drews, A.; Ferrer-Montiel, A.; Klenerman, D.; Korchev, Y. E. Local Delivery of Molecules from a Nanopipette for Quantitative Receptor Mapping on Live Cells. *Anal. Chem.* **2013**, *85*, 9333−9342.
(77) Cock, P. J. A.; Antao, T.; Chang, J. T.; Chapman, B. A.; Cox, C. J.; Dalke, A.; Friedberg, I.; Hamelryck, T.; Kauff, F.; Wilczynski, B.; de Hoon, M. J. L. Biopython: Freely Available Python Tools for Computational Molecular Biology and Bioinformatics. *Bioinformatics* **2009**, *25*, 1422−1423.
(78) Huang, J.; MacKerell, A. D. CHARMM36 All-Atom Additive Protein Force Field: Validation Based on Comparison to NMR Data. *J. Comput. Chem.* **2013**, *34*, 2135−2145.
(79) Maglia, G.; Heron, A. J.; Stoddart, D.; Japrung, D.; Bayley, H. Analysis of Single Nucleic Acid Molecules with Protein Nanopores. *Single Molecule Tools, Part B:Super-Resolution, Particle Tracking, Multiparameter, and Force Based Methods*; Elsevier, 2010; Vol *475*, pp 591−623.
(80) van der Walt, S.; Colbert, S. C.; Varoquaux, G. The NumPy Array: A Structure for Efficient Numerical Computation. *Comput. Sci. Eng.* **2011**, *13*, 22−30.
(81) McKinney, W. Data Structures for Statistical Computing in Python. *Proceedings of the 9th Python in Science Conference*, Austin, Texas (https://conference.scipy.org/scipy2010/); 2010; pp 51−56.
(82) Newville, M.; Stensitzki, T.; Allen, D. B.; Ingargiola, A. *LMFIT: Non-Linear Least-Square Minimization and Curve-Fitting for Python*; 2014; https://zenodo.org/record/11813, zenodo, DOI: 10.5281/zenodo.11813.

DOI: 10.1021/acsnano.8b09137
ACS Nano 2019, 13, 9980−9992